Dynamics of Acoustic Forcing on Turbulent Flames

A Proposal Presented to the Academic Faculty in Partial Fulfillment of the Requirements for the Degree of Bachelor of Science in Aerospace Engineering with Research Option

Author:.....

Hsin-Hsiao (Jim) Ma
Undergraduate Student
School of Aerospace Engineering

Mentor:.....

Dr. Timothy C. Lieuwen
Professor
School of Aerospace Engineering

Reader:.....

Dr. Jeff Jagoda
Processor
School of Aerospace Engineering

Co -Mentor:.....

Sai Kumar Thumuluru
Graduate Student
School of Aerospace Engineering

School of Aerospace Engineering
College of Engineering
Georgia Institute of Technology
Atlanta, Georgia

May, 2010

Acknowledgments

The author would like to thank the Georgia Tech Combustion Lab for their endless support, the author's peers who aided in experimental and post-processing tasks: Adam Kay and Adam Hart, and finally the author's mentors: Sai Kumar Thumuluru and Timothy Lieuwen for their patience and guidance.

Table of Contents

Lists of Figures

Introduction

From 2006 – 2030 the world's energy consumption is predicted to grow 44%. In the United States, the growth is predicted to be 26% during the same time period with an average energy consumption increase of 1% per year [1-2]. The sharp increase of power consumption has fueled the world to seek cheap, efficient, and environmentally friendly ways to meet the demand. Natural-gas-fired plants are renowned for their high efficiency and less carbon-intensive footprints compared to other fossil fuels. World natural gas consumption is predicted to rise 1.6% every year from 2006 to 2030 from 104 trillion cubic feet to 153 trillion cubic feet for a grand total of 38.4% increase in consumption. In the United States, natural gas plants are expected to account for 53% of all energy additions from 2007-2030. These growth percentages also take into account new and evermore stringent emission regulations to lower its environmental footprint, revealing the resilient nature of the natural-gas-fired industry.

As these new emission regulations are enforced, the gas turbine industry has turned to lowering the combustion zone temperature to prevent thermal NOx emissions, which is the leading cause for acid rain and smog. To stifle thermal NOx emissions, the combustion zone temperature has been significantly reduced to fall under a threshold temperature by operating in lean, pre-mixed (air and fuel are mixed before combustion) conditions. The combustion process is driven by an equivalence ratio, also known as the fuel-to-air ratio. An equivalence ratio of one represents that all of the fuel and air in the combustion process are completely burned and converted to products within its chemical equation. Lean conditions represent more air molecules than fuel molecules leading to unburned air. The surplus of air cools the combustion zone keeping the temperature under the threshold temperature of 2,900°F (1,600°C). Modern

gas turbine engines operate around 2,700°F (1,500°C) unlike its predecessors at 3,300°F operating at stoichiometric (equivalence ratio of one) conditions.

Operating in lean conditions has consequently introduced instabilities into the system primarily in the form of combustion driven oscillations in pressure, velocity, and heat release. The consequences of these oscillations include thrust fluctuations, structural vibrations, enhanced heat transfer, flame blowoff or flashback, which all contribute to performance degradation, lifetime degradation, operating at lower levels, and even catastrophic failure. Combustion instabilities arise from the interaction between acoustic modes of the combustor and unsteady heat release from the combustion process. In addition, a feedback loop couples the two processes together resulting in the growth of the instability until it saturates at a limit-cycle.

Background Information

This research is motivated by instabilities [3] in lean, premixed, swirl combustors. The instabilities manifest from a coupled process between: 1) the interaction between acoustics and the flame and 2) the combustion chamber. The flame is sensitive to acoustic (pressure) oscillations, and the enclosed combustion chamber leads to acoustics reflecting from boundaries upstream and downstream of the combustor to re-impinge upon the flame. The flame's sensitivity to acoustics results in a rapidly changing flame area which consequently affects its global heat release. Rayleigh's integral [4] shown in Equation 1 is used to describe the conditions necessary to transfer energy from unsteady heat release to the acoustic field where p' is pressure oscillations and q' is heat release oscillations. The sign of this integral depends on the magnitude of the phase between p' and q' known as θ_{pq}. The integral is positive when

$$\int_t p'(t)q'(t)dt$$

Equation 1: Rayleigh's Criterion Locally

$\theta_{pq} < 90°$, which leads to constructive interference between the waves and conversely negative, when $\theta_{pq} > 90°$, leading to destructive interference. Physically, when $\theta_{pq} < 90°$, the combustion process adds energy to the acoustic oscillations, resulting in oscillations that grow exponentially, until they saturate at a limit-cycle. Thus, for instabilities to manifest, the driving force of the oscillations must be greater than dampening processes inside the combustor. These will be elaborated on later.

Combustion instabilities grow and decay due to a self-excited feedback loop that relates the downstream dynamics to the upstream region. Acoustic wave propagation is generally responsible for the feedback loop, but entropy fluctuations and vorticity also play a factor. They

reflect off boundary conditions downstream of the flame, and transform into pressure waves that propagate upstream. The amplitude of the oscillations created by the feedback loop grows exponentially until it saturates into a limit cycle. The oscillations typically occur at discrete frequencies associated with the natural acoustic modes of the combustion chamber.

Limit Cycle

To put this mechanism into simpler terms, this process is analogous to blowing air into a bottle. The geometry of the bottle determines the natural acoustic modes of the system. Blowing air into the bottle would produce a specific frequency and changing the geometry by adding water would produce a different frequency. The rate and magnitude of the air going into the bottle is analogous to the driving force inside the combustor. Blowing more air into the system would yield a higher response (louder sound) until a certain input is reached where it would no longer produce a louder sound. This point is analogous to saturation inside a combustion chamber and the location of the limit cycle.

As stated previously, for instabilities to grow the driving force of the oscillations must be greater than the damping processes. As the amplitude of the oscillations increase, they reach a point where the driving and damping forces become amplitude dependent and reach a maximum amplitude. The maximum amplitude of the system is known as the limit cycle (A_{LC}) [5-6]. Figure 1 is a pictorial representation of this system where H(A) is the driving force, D(A) is the damping force and A_{LC} is the limit cycle.

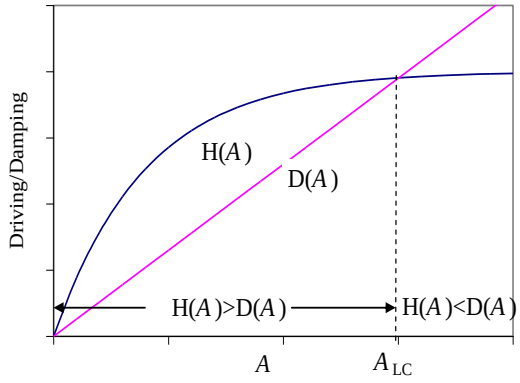

Figure 1: Qualitative plot depicting the amplitude dependence of the driving force H(A) and the damping force D(A). Adapted from [7].

The figure provided above reveals two points of interests: the origin, and the location where the driving, H(A) and the damping, D(A) intersect. These points are possible equilibrium conditions. At the origin, the equilibrium is unstable. Any perturbation to the origin would cause the system to grow linearly first then saturate to the limit cycle if the necessary forcing was present. At the limit cycle, A_{LC}, any perturbations to the system would cause the system to return to the limit cycle. Note that H(A) increases in a linear fashion when H(A) is small and then starts to saturate at a larger H(A). Saturation of the system is an onset of the amplitude dependence of the driving and damping forces. Consider the following equations:

$$H(A) \equiv \varepsilon_H A + H_n(A)$$
$$D(A) = \varepsilon_D A + D_n(A)$$

Equation 2: Linear and nonlinear components of H(A) and D(A).

When the amplitude of the oscillations is small the driving and damping forces can be approximated by:

$$H(A) = \varepsilon_H A$$
$$D(A) = \varepsilon_D A$$

Equation 3: Linear approximation of the driving force H(A) and damping force D(A).

When the amplitude is large, the amplitude dependent components of Equation 2 start to dominate and the curve changes from linear to nonlinear. The non-monotonic behavior of the system is difficult to model and identifying the culprits of this behavior is a motivator for this paper.

Instability Driving Mechanisms

The basics of instabilities are well understood, but an extensive understanding of the mechanisms causing oscillations is still an active area of research. A feedback cycle between heat release oscillations, acoustic oscillations, perturbations in flow and mixture are often responsible for self-excited instabilities. Figure 2 is provided as a pictorial representation of the feedback cycle. Fluctuating heat release produces fluctuating acoustic (pressure) oscillations

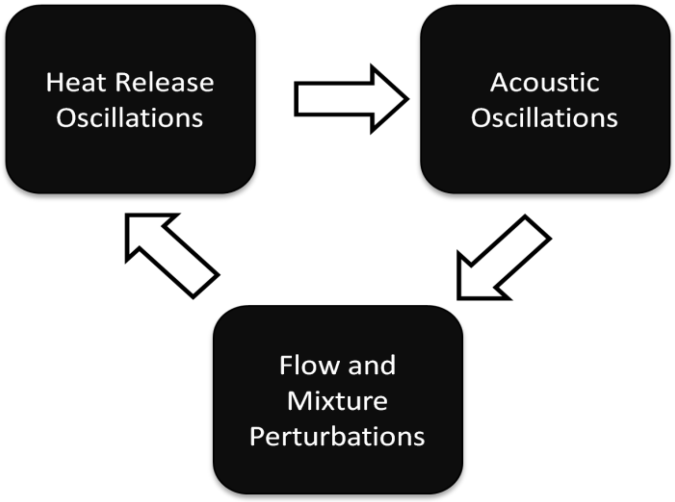

Figure 2: Feedback cycle.

that drives the acoustic oscillations. Acoustic oscillations propagate downstream and are reflected upstream to impinge upon the flame and fuel injectors. The fuel injector's fuel-spray changes shape, evaporates at different rates, and the mixing rates of the fuel vapors and air are

significantly altered under acoustic oscillations. This change in mixing alters the local equivalence ratio and changes the flame locally leading to heat release oscillations, which continues the cycle. Other mechanisms, such as vortex shedding, also play an important role in this cycle, but are not well understood. Vortical structures are commonly found in combustion chambers, and they often pull in hot products as they form before they ignite. Sudden ignition of combustion products breaks down the vortical structures leading to turbulence inside the combustion chamber. The turbulence oscillates the flame area and consequently the heat release of the flame. These mechanisms and several others can be found in detail in [8].

Damping

Damping plays an enormous role in instabilities such that the driving force must be greater than the dampening force for instabilities to occur. Some of the processes are also nonlinear, which complicates prediction and modeling efforts. The three major damping processes are: 1) viscous and heat-transfer interactions; 2) radiation and/or convection of acoustic energy; and 3) acoustic energy transferring into different acoustic modes.

Viscous and heat-transfer damping stems from transfer of acoustic energy to vortical, or entropy, perturbations. The transfer of energy generally happens at boundaries and/or due to flow separation. At a boundary, solid or fluid, the no-slip boundary condition states that the velocity of a viscous fluid must be zero relative to the boundary. This means that when acoustic oscillations hit a wall, energy must be expended to bring the velocity of the oscillation to zero relative to the surface. As a consequence, the magnitude of the incident wave is always greater than the magnitude of the reflected wave. The expended energy is converted into either vortical velocity oscillations from the no-slip boundary condition or entropy fluctuations from the temperature boundary condition. As the frequency of the oscillations increase, the magnitude of

energy dissipated increase. Dissipation due to flow separation occurs most commonly at sharp edges or rapid fluid expansion where acoustic energy is converted into vortical structures.

There are two major processes for acoustic energy to be emitted: the first process is through convection and the second is through radiation. Convection is accomplished through bulk fluid motion where the magnitude scales with the fluid's velocity. Radiation or propagation of acoustic energy is the sound emitted by the system. The magnitude of this dissipation mechanism increases with frequency.

To simply describe the combustor setup, it consists of different diameter tubes connected together. The consequence of this geometry is the resonate frequency of these tubes are contained to a small range of frequencies. Any frequencies outside of the resonate frequencies are quickly dampened while any frequencies inside are amplified. In general, acoustic energy is transferred to be either narrowband, coherent fluctuations (small range of frequencies, relatively same phase) or incoherent, broadband fluctuations (large range of frequencies, large range of phases). The latter is driven by nonlinear combustor processes. It transfers energy from one frequency into its harmonic or subharmonic frequencies. Higher frequencies are dissipated at a much higher rate as explained from the previous damping processes. Narrowband, coherent acoustic energy is transferred to incoherent, broadband fluctuations by a random Doppler shift. This occurs when acoustics are reflected or scattered from boundary conditions.

Eliminating Instabilities

Methods for eliminating instabilities fall into two major categories. The first method targets the root cause and tries to prevent the self-exciting mechanisms. The second method targets the magnitude of acoustic excitation and aims to dampen them out. All the methods presented have been successfully implemented.

The first method can be broken down into three successfully implemented techniques. The first technique was to physically move the fuel injection point such that the product of $fT_{convect}$ is outside of unstable regions where f is frequency and $T_{convect}$ is the time needed for a fuel packet to travel from its injection point to being burned. If $fT_{convect}$ forces the flame's heat release oscillation to be in phase with the pressure oscillations then from the Rayleigh's criterion, the amplitude of oscillations will grow. Note that $T_{convect}$ also has a lag term that stems from flow and mixing oscillations such that the real $T_{convect}$ is always changing. Moving the fuel injection point alters $T_{convect}$ and thus unstable regimes could be avoided altogether. The second technique focuses on stabilizing the flame to prevent large amplitude oscillations in heat release. This is done by using a pilot flame, a small flame that uses partially premixed fuel and air. The downside to this approach is it results in higher emissions due to the pilot. The third and last technique focuses on tuning fuel supply lines to inject fuel such that the heat release is out of phase with pressure oscillations.

The second method uses Helmholtz resonators to dampen out target frequencies. They're composed of a small diameter pipe and a large volume. Changing the pipe length or volume would yield a different Helmholtz frequency. The amplitude of acoustic oscillations can be greatly reduced by turning the resonant frequency of the resonator to coincide with the instability frequency.

Most manufacturers use a combination of these methods to prevent large amplitude oscillations inside combustors. In a real-world environment, ambient pressure, temperature, and density changes daily and their effects on the system could render some of these methods useless which results in ad-hoc solutions that are not fully understood [2, 9].

Problem Statement

Upgrading and installing modifications to prevent large amplitude instabilities has been commonly performed to prevent damages, but modeling techniques are needed to design a new generation of combustors that does not suffer from the same problems. Creating models to predict whether the combustor is operating in unstable conditions requires an in-depth understanding of three instability characteristics listed from easiest to hardest: 1) oscillation frequency, 2) conditions under which oscillations occur, and 3) limit-cycle amplitude. Oscillation frequency is the simplest because it requires only an understanding of the combustor's geometry, while the limit-cycle amplitude requires an understanding of the non-linear system dynamics. The last two characteristics are significant motivators for this research.

Predicting the frequency of instability oscillations is a relatively mature area. In general, only the geometry of the system and average temperature distributions are needed to provide accurate predictions. Some problems still remain such as understanding interactions of the acoustic boundary layers of the combustor and the impact unsteady heat-release has on predicting instability frequencies. Overall however, this area is mature and has already been accurately modeled.

An extensive amount of research in this area has been performed in predicting and understanding the interactions between the flow and mixture disturbances with flame and damping processes. Recently, several gas turbine companies have reported success in determining the frequency of oscillations, acoustic modes, and conditions under which oscillations occur, but research to understand the fundamental driving forces of instabilities in order to create and verify models are still under-developed. In addition, several modeling studies have treated the flame response as linearly increasing with velocity perturbation amplitude

before saturating at some prescribed amplitude [5, 10]. Also, most experiments to date have studied flame dynamics under limit-cycle amplitudes. Consequently, the mechanisms observed under limit-cycle amplitude do not suggest that those mechanisms are responsible for the onset of instability, but that they exist once the flame is unstable.

The hardest characteristic to predict is the limit-cycle amplitude, due to the difficulty of nonlinearity. Numerous mechanisms have been proposed that attempt to explain nonlinear flame dynamics and these include local/global extinction of the flame [11], nonlinear boundary condition [10], equivalence ratio perturbation [12], and flame front kinematics[13]. However, there have been very few experimental efforts that have characterized nonlinear flame response to flow perturbations [14-15]. Characterizing flame response is of specific interest because it would help designers predict whether or not a combustor could operate in certain regimes of disturbance amplitudes. Approaches can then be taken to decrease the amplitudes to acceptable ranges or to consider other design approaches to avoid these regimes.

Specifically, this research will focus on characterizing a transfer function and identifying physical mechanisms of a lean pre-mixed swirl flame and a Bunsen Burner. The experimental setups are presented below. Before running the flame experiment, a method for measuring acoustic velocity must be verified. If these goals are accomplished in time, the focus of this research will shift into acquiring extensive data from the same swirl flame setup and a turbulent Bunsen setup and any necessary post-processing. If this data is collected within the timeframe of this research, an attempt will be made into categorizing major mechanisms of the swirl flame.

Experimental Setup

Three setups were used throughout this investigation. The first two setups are combustion setups and the last setup is an impedance tube. The first setup, the swirl stabilized combustor, investigates complex flame and fluid interactions in a very turbulent environment that closely mimics real-world operating conditions. The second setup, the Bunsen burner, investigates flame and fluid interactions in a simpler combustor to isolate fundamental trends and processes. The third setup, the impedance tube, investigates the accuracy of a popular method that measures acoustic velocity. This method, the Discretized Euler method, is used in the swirl combustor. Quantifying the accuracy, limitations, and how noise affects the method plays an important role in interpreting the results from the swirl combustor.

Swirl Stabilized Combustor

The swirl stabilized combustor has a center-body that operates at atmospheric pressure at 10-20 KW thermal power. Figure 3 is a schematic of the combustor setup. The center-body is a physical body that contains the swirler with a 40° swirl angle, the ducts leading from the swirler, and is the body the flame sits on. The flow is first past through the swirler and expanded into a quartz tube of 70 mm diameter and 190 mm length. The specific length was selected to avoid a range of natural frequencies and thus, prevent any self-excited oscillations. The swirl stabilized flow provides a toroidal flow structure that has stabilizing properties. The fuel (natural gas) and air were premixed upstream of a choke point to prevent fuel/air oscillations.

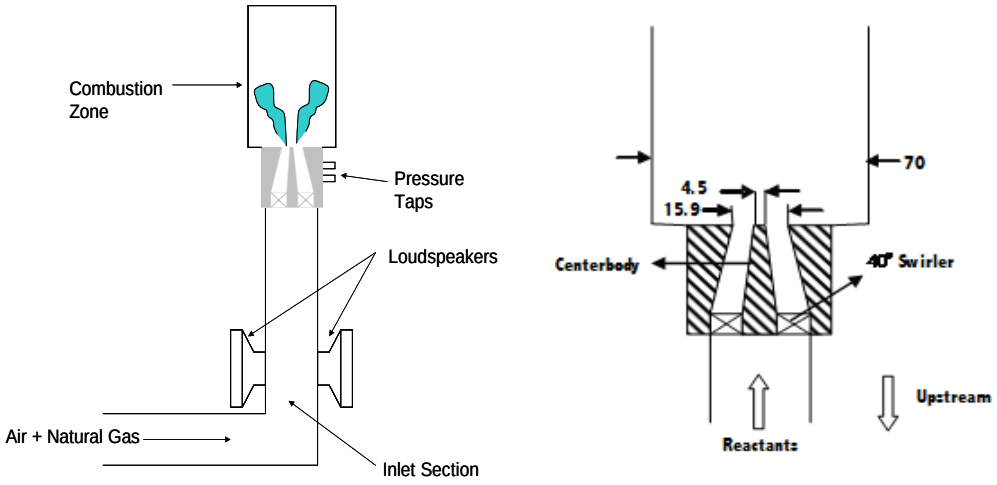

Figure 3: Combustor schematics. All dimensions are in mm

Acoustic oscillations were introduced using a function generator (Agilent 33120A Function/Arbitrary Waveform Generator), two amplifiers (Radio Shack MPA – 101 100 Watt), and two drivers (SK144 100 Watt speakers), which were mounted upstream of the combustor. Two pressure transducers (Model 211B5 Kistler) were positioned at 7 cm and 5.85 cm upstream of the nozzle. The pressure transducers were used to determine the acoustic velocity at the nozzle exit using the two microphone method [16].

Phased locked OH Planar Laser Induced Fluorescence (PLIF) was used to visualize the spatial dynamics of the flame. A schematic of the laser system is provided in Figure 4. Heat release fluctuations were characterized by measuring CH* and OH* radical emissions with photomultiplier tubes (PMTs). The PMTs were fitted with a 10 mm bandwidth filter centered at 430 nm (CH*) and 310 nm (OH*) with the field of view range covering the entire combustion region. The PLIF system used an *Nd: YAG* laser, a dye laser, and a high-resolution intensified charged-coupled device (ICCD) camera. More detailed specifications can be found in [17].

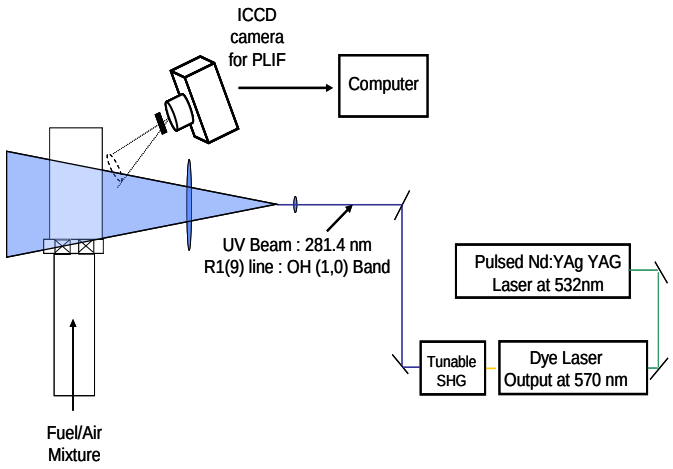

Figure 4: Schematic of OH PLIF setup. Adapted from [18]

Experiments were conducted by exposing the flame to acoustics at a selected range of frequencies, amplitudes, and phases. A typical frequency set would have six amplitudes and each amplitude would have eight phases. Each phase consists of 50 flame images at a resolution of 270 μm/pixel. These images were then post-processed to correct for heterogeneous laser intensity and noise. The flame front edges were then manually digitized before further post-processing. Different Reynolds numbers were tested by changing fuel and air flow rate, but the equivalence ratio, also known as the air-to-fuel ratio, was kept at a constant 0.8 through all experiments.

Bunsen Burner

The second combustor setup used an axisymmetric Bunsen burner with an inner diameter of 25.4 mm. The flame was stabilized by a lean premixed pilot flame using approximately 2% of the total mass flow rate. The fuel (propane or natural gas) and air were premixed upstream of the combustor. A schematic of the system with its laser system is provided in Figure 5. Acoustic oscillations were introduced using a speaker (SK144 100 Watt speakers), mounted upstream of the combustor. The Bunsen setup used the same amplifier and function generator as the swirl

stabilized combustor. Turbulent characteristics of the flow were measured using hot wire anemometry [19] at a sampling frequency of 10 kHz.

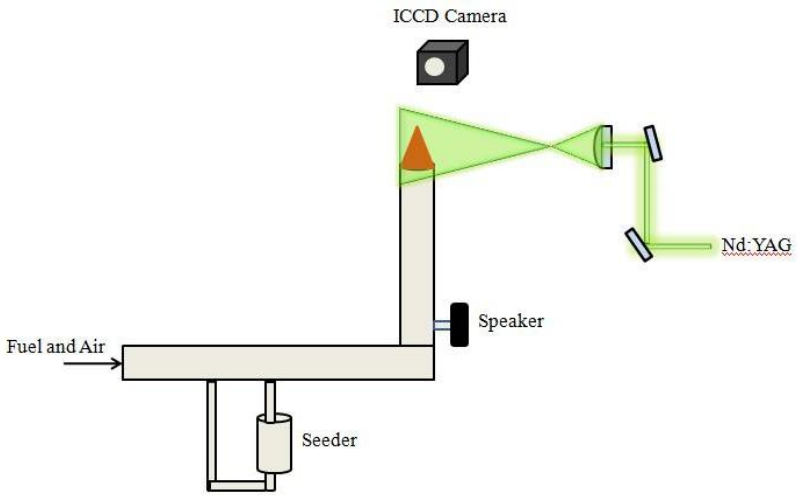

Figure 5: Schematic of Bunsen burner setup

Particle image velocimetry (PIV) was used to capture spatial characteristics and the velocity field of the flame. PIV was chosen because of its non-intrusive ability to accurately measure flow velocity. The light source was a dual-cavity, frequency doubled pulsed *Nd: YAG* laser (Surelite 1-10 PIV) with a maximum pulse energy of 110 mJ (at 532 nm) with a duration of 9 ns. Phase locking and triggering laser pulses were achieved using a delay generator (Stanford Research Systems DG-535) to synchronize the laser heads, camera shutter, and function generator. The premixed flow was seeded with aluminum oxide particles of size 2.2 μm. Scattered light from the aluminum oxide particles was captured using an interline CCD camera (Micro Max) installed with a 50 mm *f*/1.8 Nikon lens. The resolution of the camera was 1300x1030 pixels where each pixel was 6.7 μm, with a 12-bit signal resolutions resulting in a spatial resolution of 500 μm/pixel. The optics used include: a cylindrical lens (50 mm focal length, 25.4 mm diameter) that was used to expand the laser into a 3-D plane and a spherical lens (500 mm focal length, 90 mm diameter) that was used to compress the laser into a narrow,

almost 2-D laser sheet with a thickness of approximately 400 μm. The laser sheet illuminated seeded particles along the center axis of the Bunsen burner base.

Similar to the swirl burner, acoustics were varied through a range of frequencies, amplitudes, and phases. Each amplitude has eight phases. At each specified frequency and amplitude, 400 phased locked images were captured. Background noise was filtered with a 3-pixel width Gaussian filter. The velocity field was calculated using a 64 pixel square window, with a 50% overlap. A range of Reynolds numbers were tested, but all experiments were conducted at a constant equivalence ratio of 0.85.

Impedance Tube

The third setup, an impedance tube was composed of two major sections, the acoustic resonating section and the flow section as shown in Figure 6 [20]. The flow section is a one inch in diameter copper tube with a length of 13 inches. The test section is a block of aluminum with a width, height, and length of 3x3x7 respectively with all units in inches mounted along the flow section. The pressure sensors (Kistler "Piezotron" Type 211B5 piezo-electric pressure transducers) were installed four and five inches from the upstream side of the test section. The hotwire (DANTECH Dynamics 55 P11) was mounted in between the two pressure sensors. The acoustic resonator section was a two inch pipe with a length of 59 inches that opened up into the room. Two speakers (Galls SK144) were mounted in the acoustic section driven by a function generator (Agilent 33120A Function/Arbitrary Waveform Generator). Two signal conditioners were used to remove noise from the pressure sensors.

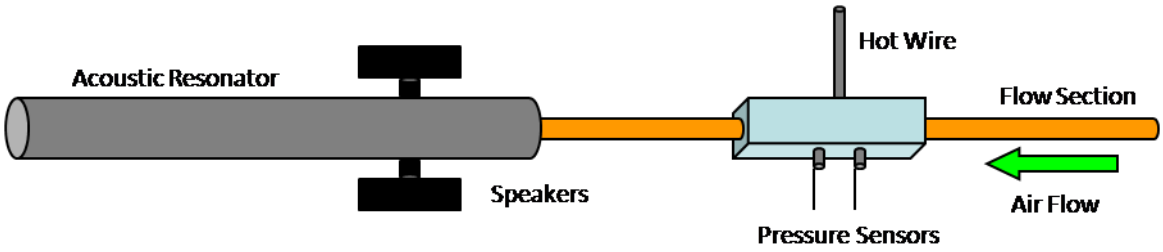

Figure 6: Schematic of the Impedance Tube [20]

A sweep of amplitudes and frequencies were conducted in this experiment. For each specified frequency, a small range of amplitudes were examined. Two Reynolds numbers were investigated: 1) 8,900 at Mach 0.028 and 2) 24,750 at Mach 0.079. The pressure sensors used the two microphone method to calculate acoustic velocity and the hotwire calculated flow velocity. The data from these two sources were compared against each other to determine the relationships between the Discretized Euler method vs. hotwire and the Plane Wave method vs. hotwire. It should be noted that this experiment could not be validated without flow because the hotwire requires a bias flow.

Results and Discussion

To aid in the interpretation of the results presented in this section, an understanding of key flame and fluid mechanical characteristics of the swirl flame combustor are presented and summarized in Figure 7. Figure 7 (a) identifies major fluid mechanical regions. In Figure 7 (a), there are four major regions of the swirl combustor and they are the inner recirculation zone (IRZ), the outer recirculation zone (ORZ), the annular jet, and finally the annular shear layers that separate the annular jet from both the IRZ and the ORZ. The IRZ, also referred to as the vortex breakdown bubble, is where vortices produced by the swirling flow breakdown. The ORZ is created by the rapid expansion of the annular jet as it exits the nozzle and consequently creates a toroidal structure. The annular jet is a high velocity jet between the ORZ and the IRZ that stems from the mean velocity of the operating condition. Lastly, the two annular shear layers are created when the high velocity annular jet interacts with the slower moving air columns in the IRZ and ORZ.

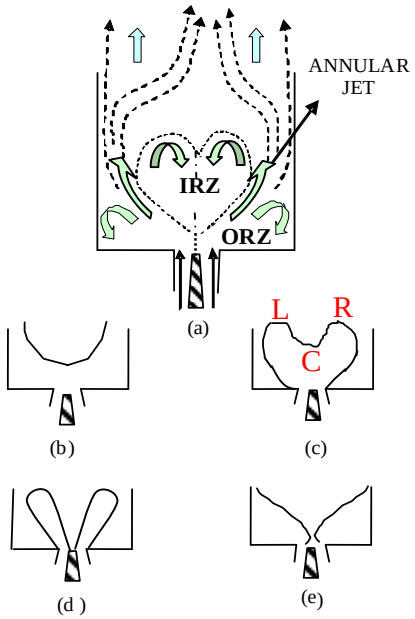

Figure 7: a) Swirl Combustor, Time Averaged Flow Field. b-e) Swirl Combustor Flame Stabilization Structures

Figure 7 (b)-(e) depicts several flame stabilization configurations. The flame stabilizes in different configurations due to physical mechanisms that start to dominate the flame's dynamics. More details on physical mechanisms are presented in the physical mechanisms sections. The physical mechanisms are typically governed by operating conditions such as equivalence ratio and flow velocities. For example, Figure 7 (c) is dominated by physical mechanisms in the IRZ such as the vortex breakdown bubble. However, the vortex breakdown bubble dominates only at a very select flow velocities. Overall, physical mechanisms that alter the behavior of the flame's stabilization configuration will drastically change how the flame behaves.

Error Analysis of the Two Microphone Validation

The two microphone technique is a non-intrusive method of measuring the acoustic velocity in a flow. The acoustic velocity is measured by assuming the acoustic form is that of a plane wave or by using a discretized version of the Euler equation. The purpose of this study was to compare the two different assumptions, determine the sensitivity of error within the assumptions, and compare the acoustic velocity calculated by the two microphone technique to the measurements of a hotwire anemometer [21]. The hotwire measures the velocity of the flow using a prong that is inserted into the mean velocity. This method is intrusive and is not feasible for reacting combustion flow where the heat produced by the combustion process would melt the hotwire.

The core of the error analysis was performed by the graduate students, Jacqueline O'Connor and Sai Kumar Thumuluru, while the author operated the experiment. As a result, this section will primarily focus on the experimental procedures. Full derivations and results can be found in [20].

Experimental error stems from two sources: systematic error due to equipment calibration and random error caused by noise in the measurements. Systematic errors come in both amplitude and phase error within an acoustic cycle. The two microphone technique uses two pressure sensors which has possibility that both pressure sensors will have both amplitude and phase error. If the errors are known, they can be corrected for during post-processing. The magnitude of these errors can be diminished by careful calibration. Figure 8 illustrates the two-microphone method where L1 is the distance from a reference point to the first pressure transducer, L2 is the distance from the same reference point to the second transducer, and R is the radius of the pipe.

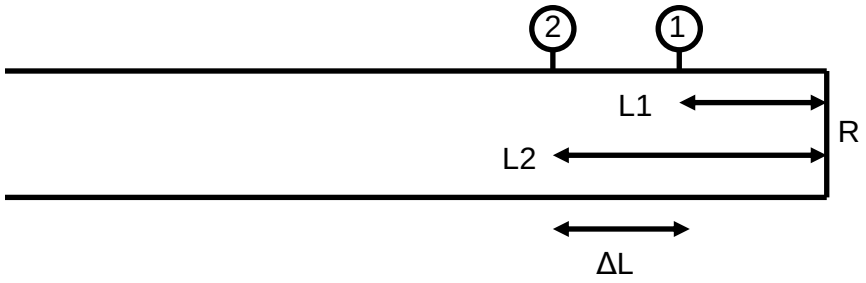

Figure 8: Diagram of Two-Microphone Method

The full experimental setup can be found in Figure 6. Before each experiment, the hotwire was calibrated since the accuracy is highly dependent on ambient temperature and pressure at the time of its calibration. Once calibrated, the data acquisition hardware was activated for the two microphones (pressure transducers) and the targeted frequency and amplitudes would be introduced into the system. The typical procedure was to target a frequency, perform an amplitude sweep from 100 mV to 1.5 V and back down to 100 mV in steps of 100 mV. This process would repeat itself for all interested frequencies.

Results from this study indicate that if operating at conditions where there are high random errors (noise), then the discretized Euler method would be advantageous. If operating

conditions include a large mean flow, then the planar wave method is most advantageous. Due to high random errors in reacting flows, the discretized Euler method will be used for future flame experiments.

Flame Transfer Function

A transfer function is a relationship between the inputs and the outputs of a system. The flame response (output) was measured at several flow velocities, forcing frequencies, and amplitudes (inputs). The flow velocities investigated were 21, 30, and 44 m/s which correspond to nozzle exit Reynolds numbers of 21,000, 30,000, and 44,000, respectively. The flame response was obtained at each flow velocity over a set of frequencies and amplitudes using OH* and CH* chemiluminescence.

OH* and CH* are produced by the flame during the combustion process and the magnitude of either quantity can be related to the heat release. Therefore, the larger the amount of OH* or CH* detected, the larger the heat release is at that location. The results for OH* and CH* followed the same trend, therefore only the results from CH* chemiluminescence is presented. Note that due to nonlinearities, the flame also responds to harmonics of the forcing frequency.

Three sets of images, one for each flow velocity is presented below. Each set has two images where the first image is a 3-D map of the topological character of the flame and the second image is the flame response. The 3-D topological map includes 2-D interpolation to fill in the surface, but the 2-D flame response map contains only experimental data. The quantity *CH*'/CH** is the magnitude of CH* fluctuation divided by the mean CH*.

Similar to *CH*'/CH*,* the quantity u'/u_o is a measure of velocity oscillations divided by the mean velocity. Therefore the larger the ratio, the stronger the velocity oscillations, but note

that the attainable u'/u_o value decreases because u' stays roughly constant even with an increasing u_o.

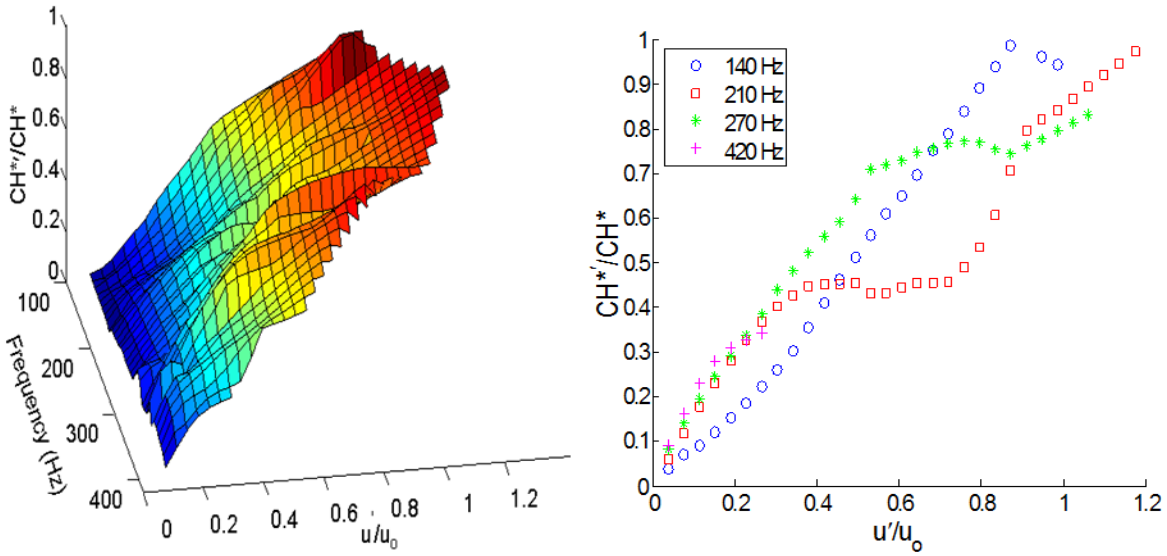

Figure 9: Topological Map and Flame Response at Flow Velocity = 21 m/s, Re = 21,000.

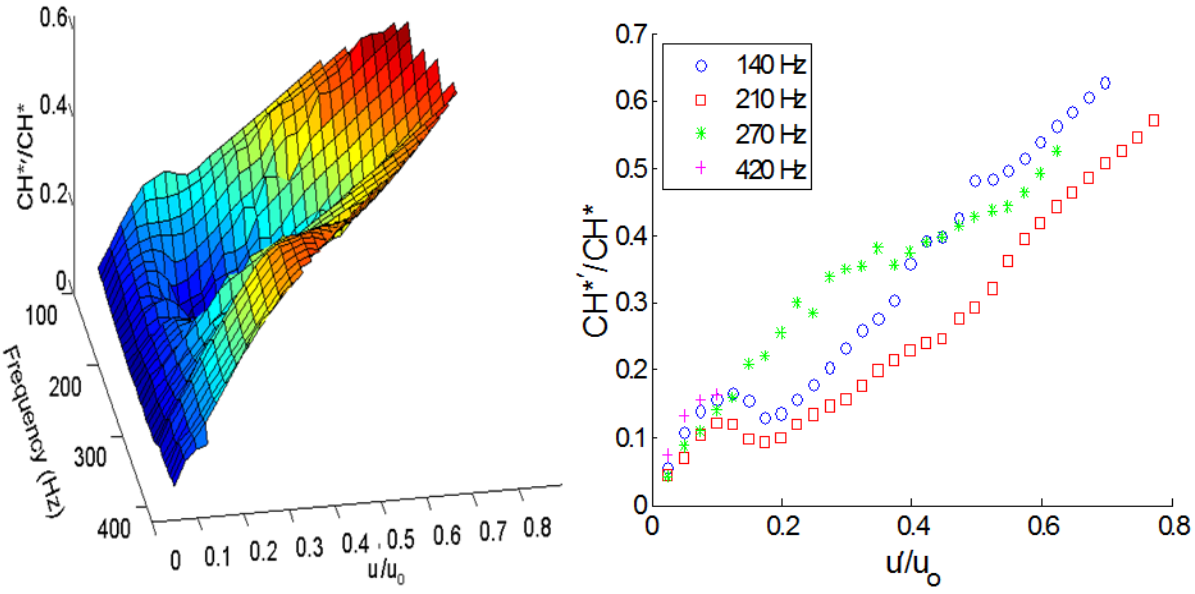

Figure 10: Topological Map and Flame Response at Flow Velocity = 30 m/s, Re = 30,000.

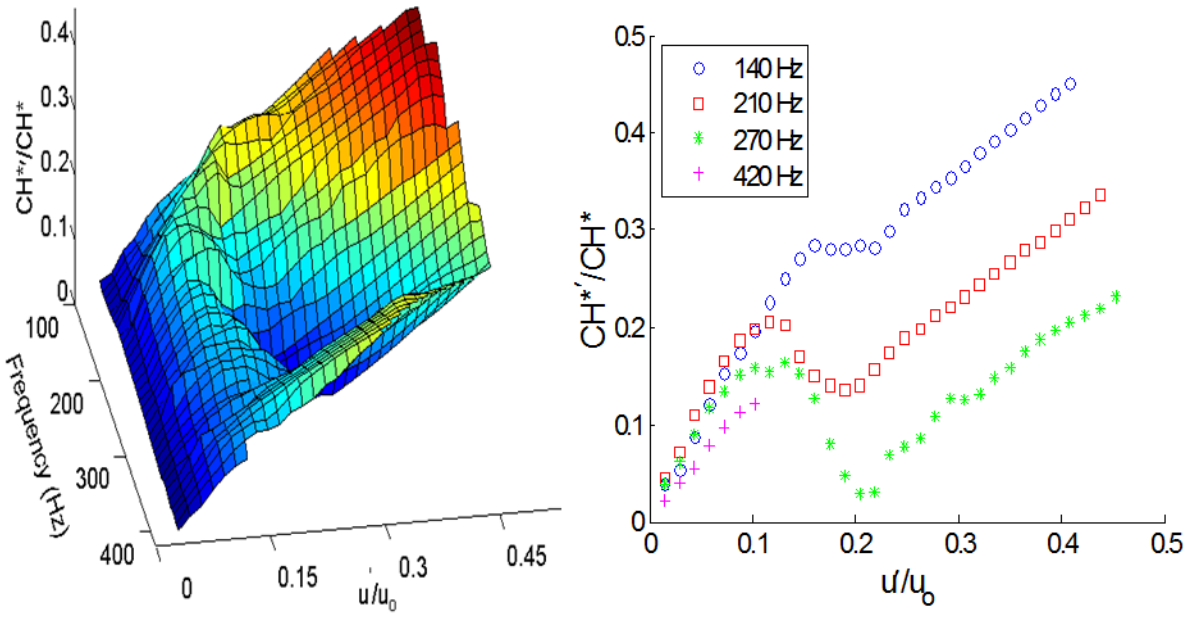

Figure 11: Topological Map and Flame Response at Flow Velocity = 44 m/s, Re = 44,000.

The following discussion will only call on the 2-D flame response figures at each flow velocity. Figure 9 shows the flame response at 21 m/s flow velocity which normally exhibits a flame shape shown in Figure 7 (d). Initially, the flame response grows linearly with increasing flow forcing, but is followed by saturation in the chemiluminescence levels ranging from 40 – 100% of its mean values. In addition, at 210 Hz, the flame response grows linearly, saturates, and then continues to grow. Presumably, the flame response would saturate at even higher amplitudes not attainable with this experimental setup.

Figure 10 depicts the flame response at a flow velocity of 30 m/s, which normally exhibits a flame shape shown in Figure 7 (c). First, notice the difference in flame shapes between the 21 m/s case and the 30 m/s case. The 30 m/s case is not attached to the inner center body which suggests that different physical mechanisms control the flame dynamics. In this case, the vortex breakdown bubble will most likely dominate its flame dynamics. Examining Figure 10, the flame response grows linearly at first, then decreases and finally increases again. The

decreasing response was not expected because it suggests that *increasing forcing amplitude causes a decreasing flame response*. Also note that the flame response does not hint at the 21 m/s trend where the flame response saturates/decreases, grows, then followed by another saturate/decrease in flame response. Again, this could be constrained by our experimental setup.

Figure 11 depicts the flame response at a flow velocity of 44 m/s, which normally exhibits a flame shape shown in Figure 7 (c). The primary difference between the 30 m/s case and the 44 m/s case is a shift in the frequency regime that exhibits the decreasing flame response, and the magnitude of the decreasing flame response. First notice in Figure 10 that 140 Hz and 210 Hz are the frequencies that have a decreasing flame response, but in Figure 11, 210 Hz and 270 Hz have decreasing flame responses, and 140 Hz saturates. Next in Figure 11, nonlinear effects play a more significant role and can be seen decreasing the flame response to a lower magnitude than in the 30 m/s case.

Overall, the 21 m/s flame response was observed to be fairly linear with amplitude while the 30 and 44 m/s case was observed to be non-monotonic with amplitude. These results suggest that the forcing frequency has a significant effect on both the linear gain and the initial saturation amplitude.

Physical Mechanisms

The goal of this study is to identify key mechanisms that influences flame dynamics. This was done by tracing the changes in the flame structure using OH PLIF images. Each image was recorded and analyzed at specific conditions within the range of: (1) frequency: 100 Hz to 410 Hz and (2) excitation amplitude: 100 mV to 1500 mV. The interpretation of these images is limited by the fact that they are only two-dimensional projections of a highly three-dimensional flow, offering only a sliver of the combustion zone. This limited view into the combustion zone

only reveals interactions on a two dimensional plane, while the flow is changing and interacting three dimensionally. Also, despite the images being phased locked, the images are actually taken several cycles apart and do not represent consecutive cycles.

A typical set of PLIF images of a flame were taken at six different phases of an acoustic cycle at selected excitation amplitudes (produced by the speakers) as shown in Figure 12 [7]. The forcing frequency here was 140 Hz at a Reynolds number of 44,000, and the phase angles correspond to phases in an acoustic cycle. The flame shape at this condition is similar to Figure 7 (c) where the flame is attached on the outer walls. Note the nozzle exit is located at the bottom of each image.

Figures 12 (a) and (b) are snapshots of the flame at low excitation amplitudes which would fall under the linear regime of the flame response. Notice that in the IRZ region, the flame is almost attached to the center-body. The significance of this phenomenon is explained later in this section. Figure 12 (c) and (d) show the flame under large excitation amplitudes where the flame response saturates and recovers, respectively. In Figure 12 (d) specifically, the flame edge in the IRZ region is far away at phase angle 120^0, stabilizes at phase angles 180^0 and 240^0, and recovers at 300^0. In general, Figure 12 provides an illustration of the flame as it surges back and forth axially, due to oscillating flow velocity in the annular jet region shown in Figure 7 (a). A closer look into this phenomenon is well illustrated in Figure 12 (d). As the excitation amplitude grows, the overall level of fluctuation of the flame length grows, which can be seen in the ORZ region as the flame edge shifts axially.

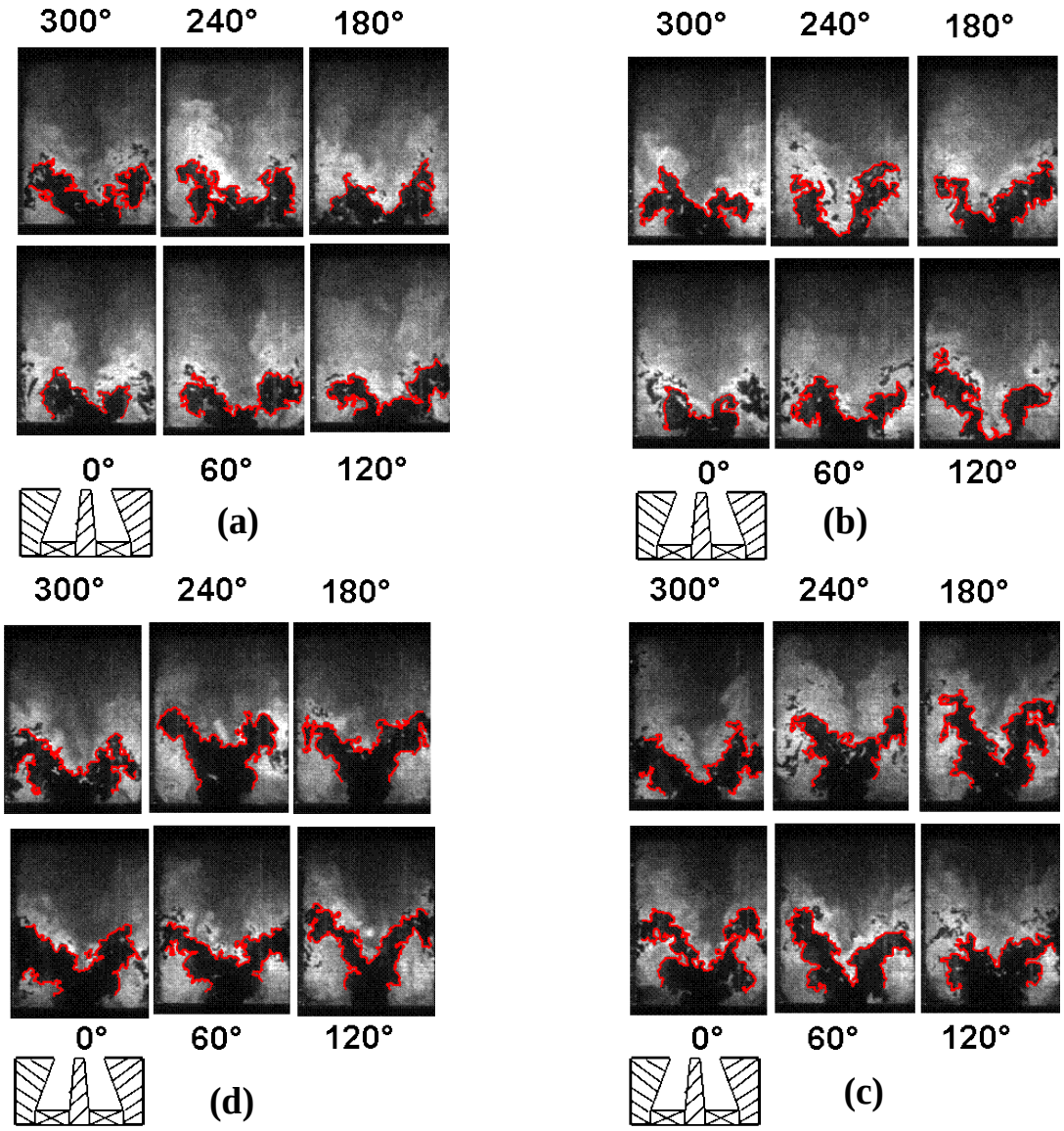

Figure 12: OH PLIF images showing flame structure at the forcing frequency of 140 Hz, Re=44,000 and amplitudes of (a) u'/u_o = 0.07, (b) u'/u_o = 0.1, (c) u'/u_o = 0.17, & (d) u'/u_o = 0.24.

Applying this process of image analysis over a range of conditions, it was observed and cataloged that there are five basic flame and/or flow processes. These processes are the following:

(1) *Fluctuating annular jet velocity* – Oscillations in flow velocity causes perturbations in the jet flow velocity between the IRZ and ORZ, causing a fluctuation in flame length.

(2) *Vortex rollup* – The oscillating shear in the inner and outer re-circulation zones generates vortical structures whose strength and size are a function of the perturbation amplitudes. These vortices roll up the flame and cause rapid destruction of the flame

area. Figure 13 [7] illustrates that significant vortex rollup occurs in both the IRZ (left) and the ORZ (right). Figure 12 (c) shows the evolution of a vortex rollup through a cycle of phase angles.

(3) *Unsteady Liftoff* – The flame's stabilization point is heavily dependent on the excitation amplitude and can be pushed downstream. At higher excitation amplitudes, the flame extinguishes locally between the swirler exits as shown in Figure 14 and re-stabilizes downstream. Notice, at 0° phase angle, the flame edge is clearly attached to the center-body while at 225° phase angle the flame edge has completely lifted off. The bulk of the heat release has moved away from the IRZ and towards the walls of the combustor. This phenomenon is apparently the cause of the saturation (non-linear regime) of the flame response to excitation. When the flame is attached to the center-body as shown in Figure 7(d) and (e), the flame edge grows linearly with excitation amplitude and stretches axially. Once the flame detaches and is blown downstream as shown in Figure 7(b) and (c), the flame responds to the higher excitation amplitude by shifting up and

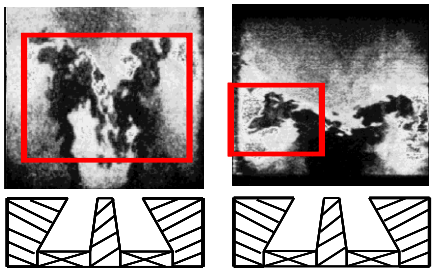

Figure 13: PLIF images showing vortex rollup in IRZ (left) and ORZ (right) at forcing frequency of (a) 130 Hz, Re=21,000, u'/u_o = 0.9 & (b) 210 Hz, Re=44,000, u'/u_o = 0.2.

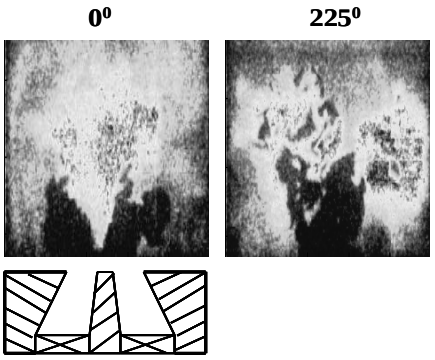

Figure 14: PLIF images showing oscillation in flame stabilization point and unsteady liftoff at forcing frequency of 410 Hz, Re=21,000 and u'/u_o = 0.6

down in bulk. This is accompanied with a decrease in flame area, which results in lower heat release.

(4) *Vortex breakdown bubble movement* – The vortex breakdown bubble, also known as the IRZ, moves up and down and changes shape with forcing, as seen in Figure 15 taken at 410 Hz. Comparing Figure 12 and Figure 15, it appears that the recirculation bubble oscillates with frequencies instead of excitation amplitude.

(5) *Turbulent flame speed oscillations* –The turbulent flame speed (speed of propagation) of the unburned reactants varies throughout the cycle of phase angles. In a previous qualitative observation described in [18], the flame topology seemed to vary with excitation amplitude. In Figure 12, where the excitation amplitudes are small, the amount of "flame wrinkling" fluctuates throughout an acoustic cycle as the excitation amplitude increases. In Figure 13 (b) and Figure 14 at a phase angle of 225^0 where the excitation amplitudes are high, the flame wrinkling becomes virtually unpredictable. This implies that the turbulent flame speed oscillates with a fluctuation level that increases with the excitation amplitude. Therefore a change in the turbulent flame speed can cause dramatic nonlinearities in the flame response.

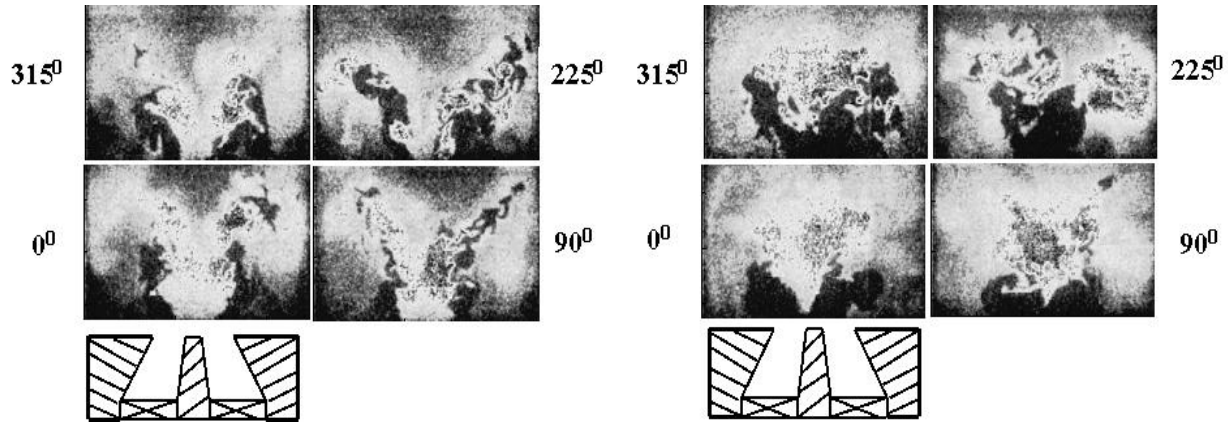

Figure 15: PLIF images at forcing frequency of 410 Hz, Re=21,000, (a) $u'/u_0 = 0.2$ (b) $u'/u_0 = 0.6$.

The Development of Turbulent Flame Brush Thickness

Turbulent flame brush thickness is a metric used to measure the transition zone between the products (burned state) and reactants (unburned state) of a premixed flame. Images were captured by the particle image velocimetry (PIV) system for the Bunsen burner setup while the swirl flame setup used planar laser induced fluorescence (PLIF). Even though two different techniques were used to capture instantaneous images, the methodology to process the data remains the same. Figure 16 and 17 are provided below as schematics of the methodology processes for the Bunsen burner and swirl flame setups, respectively.

First, a large number of instantaneous images of the flame were captured using one of the techniques above. The flame edges for each instantaneous image were then found and recorded using a manual process for the swirl flame or an automated process for the Bunsen burner and can be seen in Figures 16 (a) & 17 (a). The discrepancy between the two flame edge tracking techniques stems from the Bunsen burner's high contrast images, leading to an easier automated tracking algorithm. The second step was to superimpose all of the instantaneous flame edges for a particular experimental condition on top of each other and can be seen in Figures 16 (b) and 17 (b).

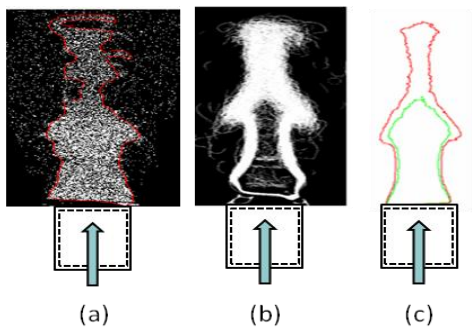

Figure 16: Bunsen Burner Flame Brush Thickness Methodology. (a) Instantaneous Flame Image with Red Line as the Flame Edge. (b) Ensemble Averaged Flame Image. (c) 0.3 (green) and 0.7 (red) Contours of the Ensemble Averaged Flame.

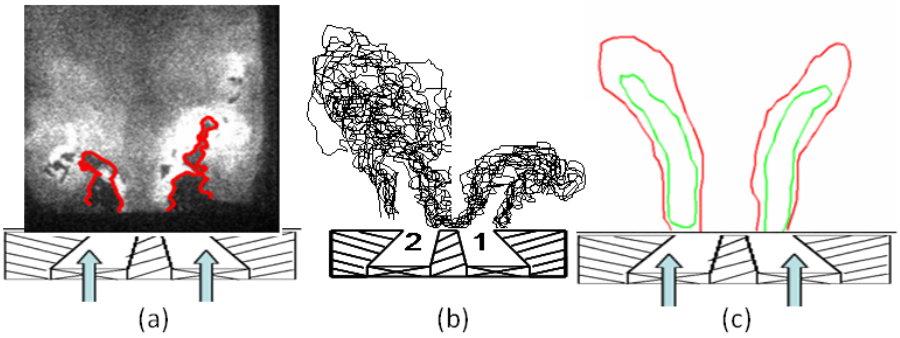

Figure 17: Swirl Flame Brush Thickness Methodology. (a) Instantaneous Flame Image with Red Line as the Flame Edge. (b) Ensemble Averaged Flame Image. (c) 0.3 (green) and 0.7 (red) Contours of the Ensemble Averaged Flame.

The final step was to quantify locations to measure the flame brush thickness. This was done through a series of steps that starts with converting each instantaneous flame image into an array of either $\bar{c}$ = 0 when there are only reactants present at that location or $\bar{c}$ =1 when there are only products at that location. $\bar{c}$ is a progress variable. Now each instantaneous flame image is a binary image with each pixel labeled as a 0 or a 1. All of these binary images are then averaged to yield an ensemble averaged image with the progress variable $\bar{c}$, ranging from 0 – 1. The distance between $\bar{c}$ = 0.3 and 0.7 is the flame brush thickness. Figures 16 (c) & 17 (c) shows the two contours with $\bar{c}$ = 0.3 on the inside (green line) and $\bar{c}$ = 0.7 on the outside (red line).

Bunsen Burner

The flame brush thickness (δ_t) was found at experimental conditions of Re = 10,200, mean flow velocity of 10 m/s at the nozzle exit, and turbulent fluctuations of u'_t/u_o = 0.05. Forced excitations were introduced into the system at f = 200 Hz, increasing the turbulent fluctuations to u'_t/u_o = 0.15. An image of the unforced ensemble average Bunsen flame is provided in Figure 18, while an image of the ensemble average Bunsen flame under acoustic excitation is provided in Figure 19.

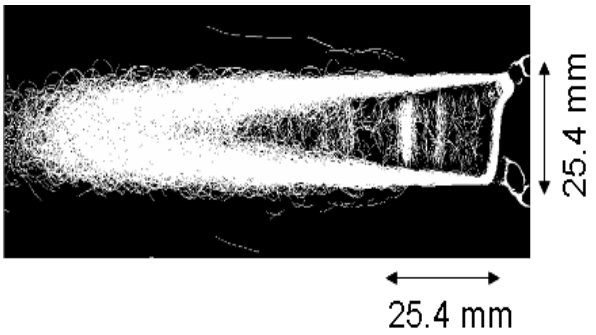

Figure 18: Unforced Ensemble Averaged Bunsen Flame

From Figure 18 & 19 the flame brush thickness can be approximated as the white brush. The white brush clearly grows as it propagates downstream (from right to left). Figure 19 depicts how the flame brush grows through phases of an acoustic cycle. Note that at a frequency of 200 Hz, the cycle starting at 0° to 315° happens 200 times a second. Figure 20 depicts how the normalized flame brush thickness (δ_t /D) grows versus the normalized flame coordinate (s/D).

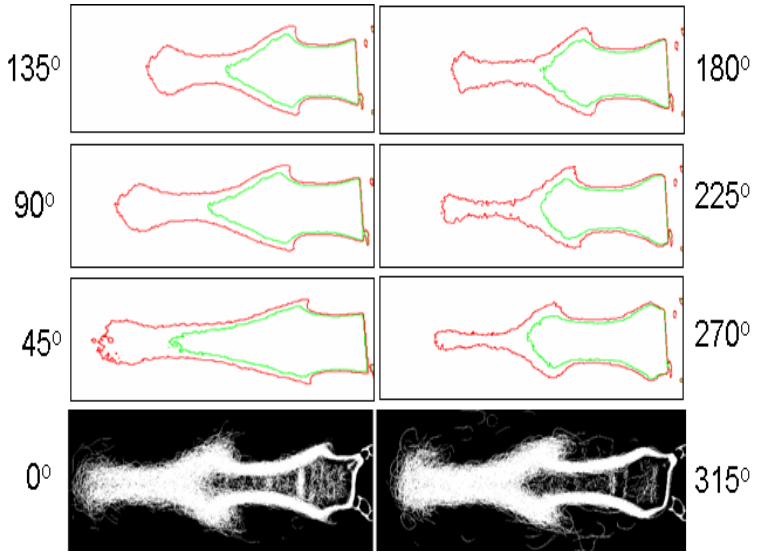

Figure 19: Flame Brush Thickness Development at Re = 10,200, f = 200 Hz, and u'/u_o = 0.15.

In Figure 20 notice how the unforced case grows in a near linear fashion. Contrasting this against the cases under acoustic forcing, the flame brush thickness grows in a step-like fashion, followed by saturation or a slower growth rate. These trends can be visually verified in Figure 19 where the flame brush thickness grows very slowly until a convecting vortex where the flame

brush thickness jumps. Downstream of the vortex, the flame brush thickness grows at a very small rate.

These results show that acoustic excitation changes how the flame behaves through different growth rates of the flame brush thickness. This suggests that the flame brush thickness under acoustic forcing evolves in a non-quasi steady manner. Also notice that the location of the convecting vortex changes with different phase angles in the acoustic cycle.

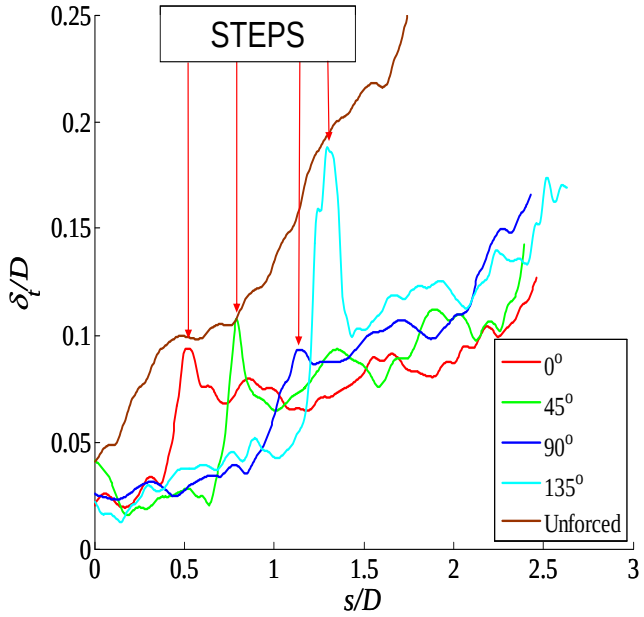

Figure 20: Normalized Flame Brush Thickness (δ_t/D) vs. Normalized Flame Coordinate (s/D)

Swirl Stabilized Flame

The flame brush thickness for the swirl stabilized flame were obtained at Re = 21,000 at the nozzle exit with a mean velocity of 21 m/s. Acoustic forcing was at f = 130 Hz and the turbulent fluctuations were maintained at u'_A/u_o = 0.6. Figure 21 depicts the development of the flame brush thickness without acoustic excitation, Figure 22 shows the flame brush thickness of the swirl stabilized flame through an acoustic cycle at f = 130 Hz, and Figure 23 plots the results of how the flame brush thickness develops versus normalized flame coordinate.

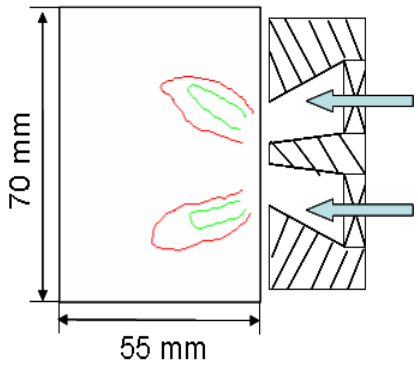

Figure 21: Unforced Flame Brush Thickness with $\bar{c}$ =0.3 (green line) and $\bar{c}$ =0.7 (red line).

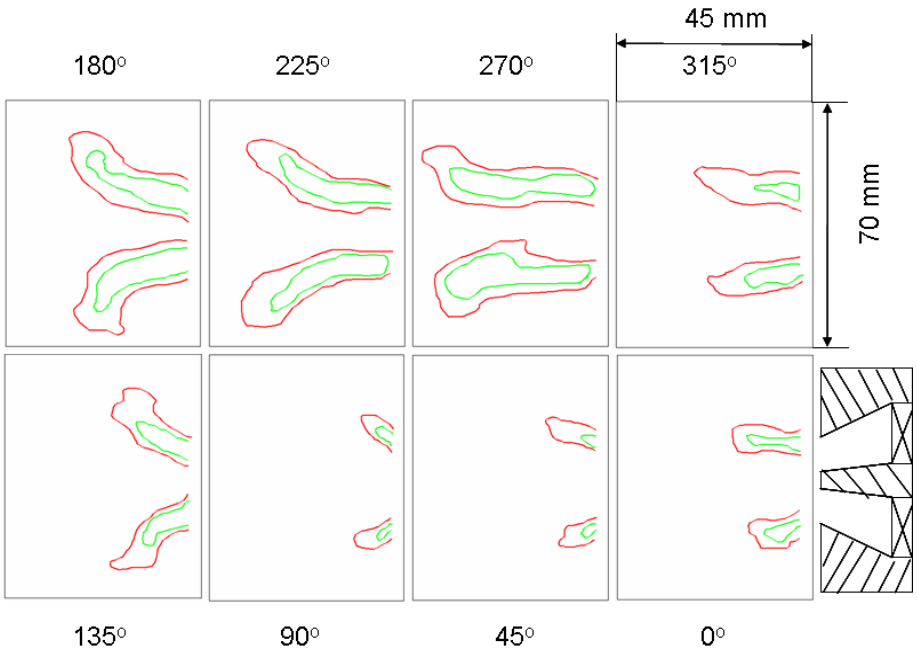

Figure 22: Brush Thickness Development at Re = 21,000, f = 130 Hz, and u'/u_o = 0.6.

Figure 22 shows how the flame length changes with acoustic phase. Notice that there is no longer a vortex that forces the flame brush thickness to grow rapidly. Correlating these observations to Figure 23, there is indeed no rapid increase in flame brush thickness, unlike the Bunsen burner setup. Next, observe how the length of each acoustic phase varies significantly. This correlates back to Figure 22, where the flame length is changing with each acoustic phase. Finally, the unforced case grows linearly similar to the unforced Bunsen burner. However, the results suggest that acoustic excitation inhibits flame brush thickness growth.

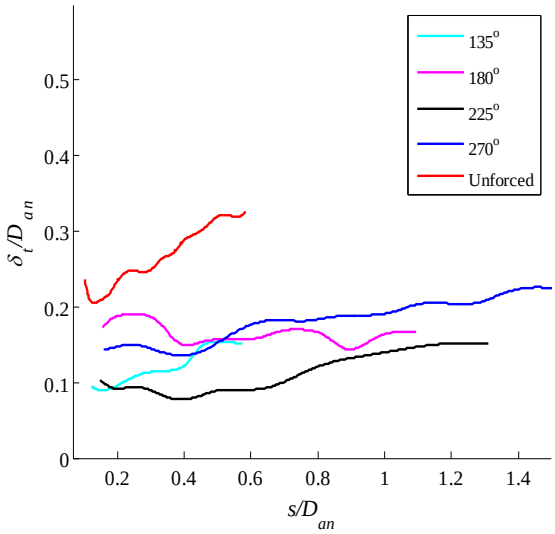

Figure 23: Normalized flame brush thickness (δ_t/D_{an}) vs. normalized flame coordinate (s/ D_{an})

The results of the two experimental setups show that acoustic forcing dramatically changes how the flame behaves. In both cases, the acoustic excitations changed the global flame behavior. In the Bunsen burner, acoustic excitation induced vortices that caused the flame brush thickness to grow rapidly. Acoustic excitation in the swirl stabilized setup actually inhibited the growth of the flame brush thickness.

Conclusion

The purpose of this study was to investigate the behavior of turbulent, premixed flames under acoustic forcing. Physical mechanisms within the flame such as vortex rollup and a fluctuating annular jet will often dominate flame dynamics leading to rapid changes in heat release. These physical mechanisms are often a function of several factors including combustor geometry, acoustic forcing, and experimental conditions. To better understand the effects of the physical mechanisms, the transfer function of the swirl flame was found by altering acoustic forcing and experimental condition – turbulence level (u'/u_o). The transfer function yielded that the flame response in some cases saturate with increasing forcing or even decrease with increasing forcing. The flame brush thickness was then found for both the swirl flame and Bunsen flame to investigate the physics of the flame in cases where the flame saturates or decreases with increased forcing. The results show that under acoustic forcing, the flame brush thickness grows in a step like fashion in the Bunsen burner case. In the swirl case, acoustic forcing actually inhibits flame brush thickness growth. It was also shown that the rapid growth of the flame brush thickness in the Bunsen burner case stemmed from a physical mechanism – vortices.

Although the results presented from this study are years from implementation, they provide the foundation for the development of the next generation of cleaner, more efficient gas turbine engines. A roadmap is provided in Figure 24 to bring this problem from the nuts and bolts of flame dynamics and back to the real world.

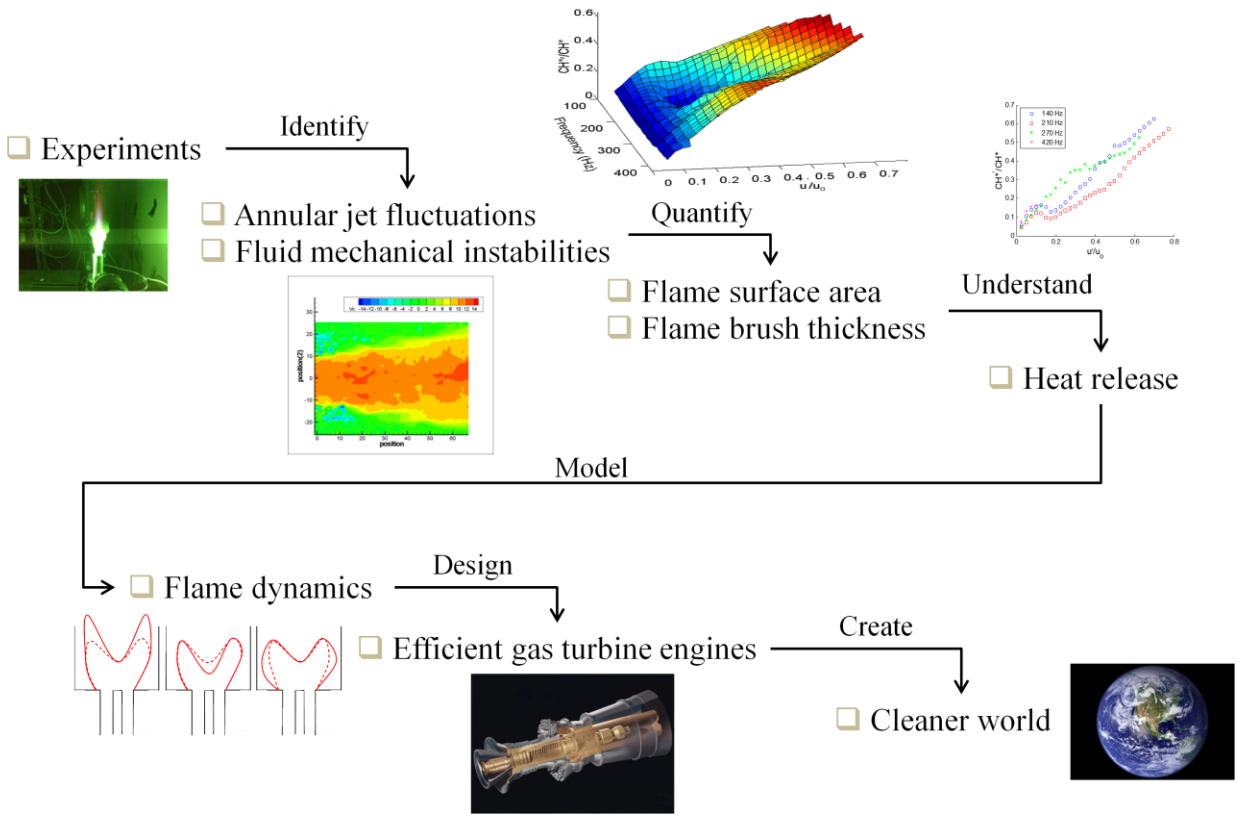

Figure 24: Flame Study Methodology

Before experiments were conducted, equipment such as the PIV, PLIF, and the two microphones technique were investigated, validated, and verified. Experiments were then conducted to identify major mechanisms that dominate flame behavior such as annular jet fluctuations and fluid mechanical instabilities. Once identified, their effects on flame properties such as flame surface area and flame brush thickness had to be quantified to understand heat release. With an understanding of heat release, a model of flame dynamics can be developed to aid engineers in designing more efficient gas turbine engines that will decrease emissions and create a cleaner world.

References

[1] J. A. Beamon, Conti, J. J., Holtberg P. D., Kydes, A. S., Schaal, M., Sweetnam, G. E., "Annual Energy Outlook 2009 with Projections to 2030," Energy Information Administration2009.

[2] G. A. Richards, *et al.*, "Passive control of combustion dynamics in stationary gas turbines," *Journal of Propulsion and Power,* vol. 19, pp. 795-810, 2003.

[3] J. G. Lee and D. A. Santavicca, "Experimental diagnostics for the study of combustion instabilities in lean premixed combustors," *Journal of Propulsion and Power,* vol. 19, pp. 735-750, 2003.

[4] J. W. S. Rayleigh, *The Theory of Sound* vol. 2. New York: Dover, 1945.

[5] A. P. Dowling, "Nonlinear self-excited oscillations of a ducted flame," *Journal of Fluid Mechanics,* vol. 346, pp. 271-290, 1997.

[6] T. C. Lieuwen, & Zinn, B. T., "Experimental Investigation of Limit-Cycle Oscillations in an Unstable Gas Turbine Combustor," *Journal of Propulsion and Power,* vol. 18, pp. 61 - 67, 2002.

[7] S. K. Thumuluru, Ma, H., Lieuwen, T., presented at the AIAA, 2007.

[8] S. Ducruix, Schuller, T., Durox, D., and Candel, S., "Combustion Dynamics and Instabilities: Elementary Coupling and Driving Mechanisms," *Journal of Propulsion and Power,* vol. 19, pp. 722 - 734, 2003.

[9] T. Lieuwen, & Yang, V., *Combustion Instabilities in Gas Turbine Engines: Operational Experience, Fundamental Mechanisms, and Modeling* vol. 210. Reston, Virgina: American Institute of Aeronautics and Astronautics, 2005.

[10] A. P. Dowling, "A kinematic model of a ducted flame," *Journal of Fluid Mechanics,* vol. 394, pp. 51-72, 1999.

[11] T. C. Lieuwen, "Experimental investigation of limit-cycle oscillations in an unstable gas turbine combustor," *Journal of Propulsion and Power,* vol. 18, pp. 61-67, Jan-Feb 2002.

[12] A. A. Peracchio and W. M. Proscia, "Nonlinear Heat Release/Acoustic Model for Thermo-Acoustic Instability in Lean Premixed Combustors," *Journal of Engineering for Gas Turbines and Power,* vol. 121, pp. 415–421, 1999.

[13] F. Baillot, *et al.*, "Experimental and theoretical study of a premixed vibrating flame," *Combustion and Flame,* vol. 88, pp. 149–168, 1992.

[14] D. Durox, *et al.*, "On the shape of flames under strong acoustic forcing: a mean flow controlled by an oscillating flow," *Journal of Fluid Mechanics,* vol. 350, pp. 295-310, 1997.

[15] A. Bourehla and F. Baillot, "Appearance and Stability of a Laminar Conical Premixed Flame Subjected to an Acoustic Perturbation," *Combustion and Flame,* vol. 114, pp. 303-318, 1998.

[16] S. Allam, & Åbom, M. , "Investigations of Damping and Radiation using Full Plane Wave Decomposition in Ducts," *Journal of Sound and Vibration,* vol. 292, pp. 519 - 534, 2005.

[17] S. K. Thumuluru, Bobba M.K., Lieuwen, T., presented at the ASME Paper, 2007.

[18] B. D. Bellows, *et al.*, "Forced response of a swirling, premixed flame to flow disturbances," *Journal of Propulsion and Power,* vol. 22, pp. 1075-1084, Sep-Oct 2006.

[19] H. H. Bruun, *Hot-Wire Anemometry Principles and Signal Analysis*. Oxford: Oxford University Press, 1995.

[20] T. O'Connor, Ma, Dasher, & Lieuwen, "Title," unpublished|.
[21] H. H. Bruun, "Hot-Wire Anemometry: Principles and Signal Analysis," *Measurement Science and Technology*, vol. 7, 1996.